Imaging lung tissue oscillations using high-speed X-ray velocimetry

Jordan Thurgood,[a] Stephen Dubsky,[a] Kentaro Uesugi,[b] Michael Curtis,[a] Chaminda R. Samarage,[c] Bruce Thompson,[d] Graeme Zosky[e] and Andreas Fouras[a]*

[a]Department of Mechanical and Aerospace Engineering, Monash University, Wellington Road, Clayton, Victoria 3800, Australia, [b]SPring-8/JASRI, Hyogo, Japan, [c]4Dx Pty Ltd, Howleys Road, Notting Hill, Victoria 3164, Australia, [d]Allergy Immunology and Respiratory Medicine, The Alfred Hospital and Department of Medicine, Monash University, Commercial Road, Melbourne, Victoria 3004, Australia, and [e]School of Medicine, University of Tasmania, 17 Liverpool Street, Hobart, Tasmania 7000, Australia. *Correspondence e-mail: andreas.fouras@monash.edu

This work utilized synchrotron imaging to achieve a regional assessment of the lung's response to imparted oscillations. The forced oscillation technique is increasingly being used in clinical and research settings for the measurement of lung function. During the forced oscillation technique, pressure oscillations are imparted to the lungs *via* the subjects' airway opening and the response is measured. This provides information about the mechanical properties of the airways and lung tissue. The quality of measurements is dependent upon the input signal penetrating uniformly throughout the lung. However, the penetration of these signals is not well understood. The development and use of a novel image-processing technique in conjunction with synchrotron-based imaging was able to regionally assess the lungs' response to input pressure oscillation signals in anaesthetized mice. The imaging-based technique was able to quantify both the power and distribution of lung tissue oscillations during forced oscillations of the lungs. It was observed that under forced oscillations the apices had limited lung tissue expansion relative to the base. This technique could be used to optimize input signals used for the forced oscillation technique or potentially as a diagnostic tool itself.

1. Introduction

Multiple-frequency forced oscillations are regularly used to probe lung mechanics in both health and disease (Oostveen *et al.*, 2003). This is typically achieved by measuring the input impedance of the respiratory system in response to multi-frequency sinusoidal pressure oscillations applied at the airway opening (Zosky & Sly, 2007). Mathematical models, which are usually based on a single compartment model of the lung (Bates & Suki, 2008), are then used in an attempt to partition the response (impedance) into parameters that represent the frequency-independent and dependent response of the central airways and lung periphery (Hantos *et al.*, 1992).

One of the most common, robust and simple of these mathematical models contains four parameters, where the lung tissue is assumed to exhibit a constant phase behaviour (Hantos *et al.*, 1992). This model allows an estimation of parameters representing: (i) Newtonian resistance (R_N), the frequency-independent resistance of the in-phase component of the impedance; (ii) inertance (I), which is related to the mass of the gas in the central airways; (iii) tissue damping (G), which describes the shape of the frequency dependence of the in-phase component of the impedance and reflects the viscous properties of the lung periphery; and (iv) tissue elastance (H),
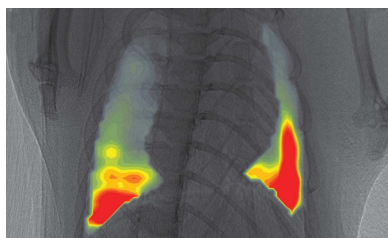
which describes the frequency-dependent elastic behaviour of the system (Bates *et al.*, 2011).

The capacity to mathematically separate responses in the central airways and lung periphery is particularly useful for examining lung mechanics in different regions of the lung. However, achieving this partitioning is dependent on signal design, in particular the frequency range that is used. This is because the penetration of the signal throughout the airways and the interaction with the lung parenchyma is frequency-dependent, such that higher frequencies do not penetrate beyond the central airways (Komarow *et al.*, 2011). Studies using the alveolar capsule technique have clearly demonstrated that the penetration of pressure oscillations applied at the airway opening decreases with increasing frequency (Frantz & Close, 1985) which, even in a healthy lung, may lead to regional heterogeneities at high frequencies (Fredberg *et al.*, 1984). While significant insights into the frequency-dependent behaviour of regional lung mechanics have been gained from such studies, such techniques are limited in their capacity to assess the regional frequency-dependent penetration of pressure oscillations over the entire lung.

The aim of this study was to utilize synchrotron-based lung imaging in combination with a novel frequency-based image analysis method to observe the penetration of a commonly used multi-frequency forced oscillation signal in the healthy mouse lung. Our observations yield insights into the potential heterogeneity of the penetration of oscillatory signals and demonstrate the utility that this novel technique can provide. This technique has implications for the interpretation of global measures of lung mechanics and could allow for the optimization of forced oscillation methods.

2. Methods

2.1. Animal procedures

Adult male Balb/c mice (n = 3; 9 weeks old) were anaesthetized with somnopentyl (pentobarbitone sodium; i.p.; 70 mg kg^{-1}) and orally intubated with a 20G endotracheal tube. Mice were then positioned upright in a custom-made imaging sample mount. Anaesthesia was maintained during imaging using a constant infusion of pentobarbitone sodium (somnopentyl; i.p.; 0.012 mg min^{-1}). Observation of the mouse using a closed-circuit camera and ECG ensured appropriate depth of anaesthesia. Several deceased mice were also imaged to assess the effect of the heartbeat, as well as to assess rigor mortis.

Ventilation was maintained with a custom-designed pressure-controlled ventilator (Kitchen *et al.*, 2010), with an inspiratory time of 135 ms at a positive inspiratory pressure of 14 cm H$_2$O, and an expiratory time of 265 ms at an end-expiratory pressure of 2 cm H$_2$O which equates to a ventilation frequency of 2.5 Hz (150 breaths min^{-1}). Ventilation was paused during forced oscillation testing and resumed immediately after the oscillations ceased. The animals were monitored during the function tests and any spontaneous breathing resulted in the test being abandoned and the animal being reimaged if possible.

All work involved in this study was approved by and performed according to the rules of Monash University's School of Biomedical Science's Animal Ethics Committee and the SPring-8 Animal Care Committee.

2.2. Forced oscillations

The forced oscillation signal was generated from a loud-speaker enclosed in a plastic box with a single wave tube of known impedance connecting the forced oscillation loud-speaker to the airway of the animal *via* the tracheal cannula (Fig. 1). The lateral pressure was measured at the start of the wave tube and at the airway opening.

A custom-designed three-dimensional printed junction was used at the airway opening to connect the inspiratory and expiratory ventilation tubes as well as the wave tube from the forced oscillation speaker. The design allowed for the wave tube to be closed off during ventilation, and for the ventilation lines to be closed during application of the oscillatory signal. The input oscillatory signal was composed of seven frequencies ranging from 2 to 20.5 Hz (Table 1), a frequency range optimized for partitioning respiratory system impedance in
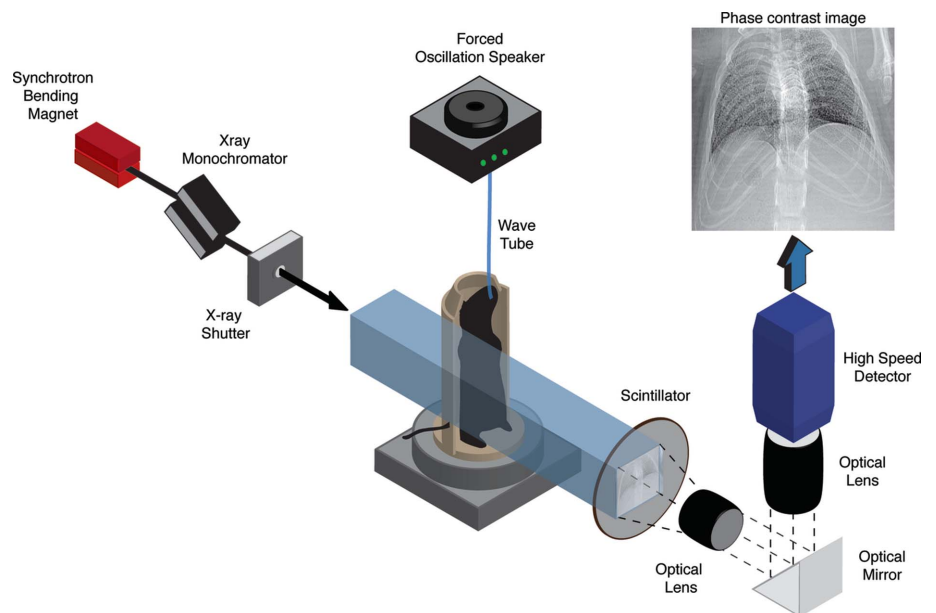
Figure 1
Configuration used to acquire images of local lung tissue expansion whilst applying forced oscillations at the airway opening. Coherent synchrotron radiation was directed through the subject impinging on a scintillator. As the X-rays were imparted onto the scintillator they were converted to visible light and directed towards a high-speed detector (PCO Edge 4.2). The detector utilized highly sensitive sCMOS technology to achieve high frame rates with low noise. The speaker and wave tube, used for imparting pressure oscillations into the respiratory system of the mice, is shown in the upper middle section of the figure.

Table 1
Frequency, relative power and phase for the input pressure oscillations.

Seven frequencies were used, designed to minimize any interaction between the harmonics of the frequencies. It can be seen that, as the frequency increased, the input power relative to the lowest frequency decreased.

Frequency (Hz)	Power (arbitrary unit)	Phase (radians)
2	1	0
3	0.667	3.388
4.5	0.444	5.811
6.5	0.308	−3.686
9.5	0.211	0.145
14.5	0.138	−5.318
20.5	0.108	2.193

mice (Larcombe *et al.*, 2013). The input oscillatory signal generated from the speaker was measured at the airway opening (Fig. 2).

2.3. Imaging setup

X-ray imaging of mice was conducted at the SPring-8 synchrotron. Synchrotrons uniquely provide both high flux and highly spatially coherent X-rays. High flux allows for high-speed imaging (Jamison *et al.*, 2012; Dubsky *et al.*, 2010, 2012) whilst high spatial coherence allows for the use of phase-contrast imaging techniques (Momose *et al.*, 1996; Lewis *et al.*, 2005; Kitchen *et al.*, 2004; Fouras *et al.*, 2009). The mice were imaged within hutch 3 of the SPring-8 BL20B2 beamline, with a monochromator used to filter the beam to an energy of 24 keV. A 25 µm-thick P45 gadolinium oxide scintillator was used to convert the X-rays into visible light. This visible light was then imaged using a sCMOS camera sensor (PCO Edge 4.2). Images were acquired at a frame rate of 100 frames s^{-1}, providing an optimum balance between image quality and temporal resolution. This high-speed imaging setup used was an adaption of that from prior studies (Thurgood, Dubsky *et*
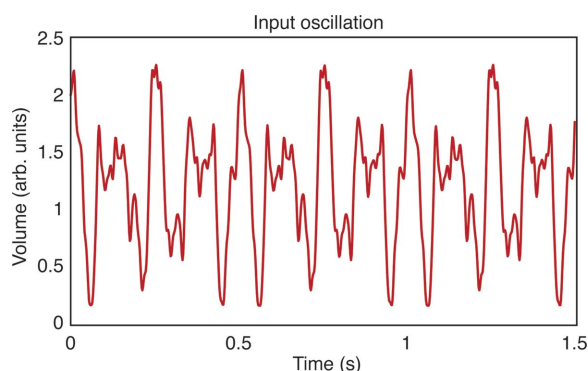
Figure 2
Volume–time curve of the input oscillation signal as measured at the airway opening. The complex waveform seen here is the result of the seven independent frequencies being generated simultaneously. These oscillations were measured at the airway opening using a custom-made three-dimensional printed restriction-based flow meter. The volume–time curve can be seen to repeat every 0.5 s correlating to the lowest input frequency of 2 Hz. Comparison of the input signal with the measured volume–time curve was performed to ensure accurate measurements at the airway opening.

al., 2012; Thurgood, Hooper *et al.*, 2012; Fouras *et al.*, 2012; Dubsky *et al.*, 2012; Thurgood *et al.*, 2014) (Fig. 1).

2.4. X-ray velocimetry

X-ray velocimetry is an emerging field in which image-processing methods are adapted from the engineering field of particle image velocimetry, and are applied to dynamic X-ray image sequences (Dubsky *et al.*, 2012; Fouras *et al.*, 2012; Thurgood, Dubsky *et al.*, 2012; Thurgood, Hooper *et al.*, 2012; Seeger *et al.*, 2001; Antoine *et al.*, 2013; Lee *et al.*, 2011). When applied to the breathing lungs, X-ray velocimetry allows for a regional assessment of lung tissue motion and can be used to derive the local lung tissue expansion and the distribution of ventilation throughout the respiratory system (Thurgood, Hooper *et al.*, 2012; Fouras *et al.*, 2009, 2012).

Images were high-pass filtered to remove the low spatial frequency structures such as ribs and other bone structures whilst isolating the high spatial frequency alveolar structures of the lung tissue. The filtered images were then divided into interrogation windows of 128×128 pixels with an 87.5% overlap between windows in both the x and y directions. An iterative cross-correlational analysis was performed on each window between subsequent frames to determine the modal displacement for that particular region of the image. Local lung tissue expansion was calculated as the divergence of the local tissue displacements measured by the X-ray velocimetry analysis (Fouras *et al.*, 2012). The tissue expansion was integrated through time to calculate the volume–time curves for each region across the lung. Determining the volume–time curves from two-dimensional X-ray velocimetry data has been described in detail in prior publications of the senior author (Thurgood, Hooper *et al.*, 2012; Fouras *et al.*, 2012).

The imaging method and image processing resulted in lung tissue expansion measurements being made at approximately 1000 locations across the mouse lung. Each imaging run consisted of 1000 frames equating to 10 s of forced oscillation input.

2.5. Frequency analysis

A volume–time curve (1000 time points) was created at each spatial location across the lung. A Fourier analysis was then performed on the volume–time curve at each location within the lung to determine the amplitude and power of lung tissue expansion that was occurring at each of the input frequencies. The global sum was taken of all the individual measures across the lung, and this global measure was then plotted (Fig. 3b) along with the frequency response for the input signal measured with a pressure sensor at the mouth (Fig. 3a). Both plots were normalized to the power of the lowest input frequency (2 Hz). The input signal, the oscillation measured at the airway opening and the imaging-based frequency responses were all binned using a 1/6 octave band to compensate for the broadening of the peak that was suspected to have occurred as a result of resonance (Fig. 3c).

The results of the Fourier analysis were visualized as maps showing the power of lung tissue oscillations at each input

(a)

Input pressure

(b)

Images lung tissue oscillations

(c)
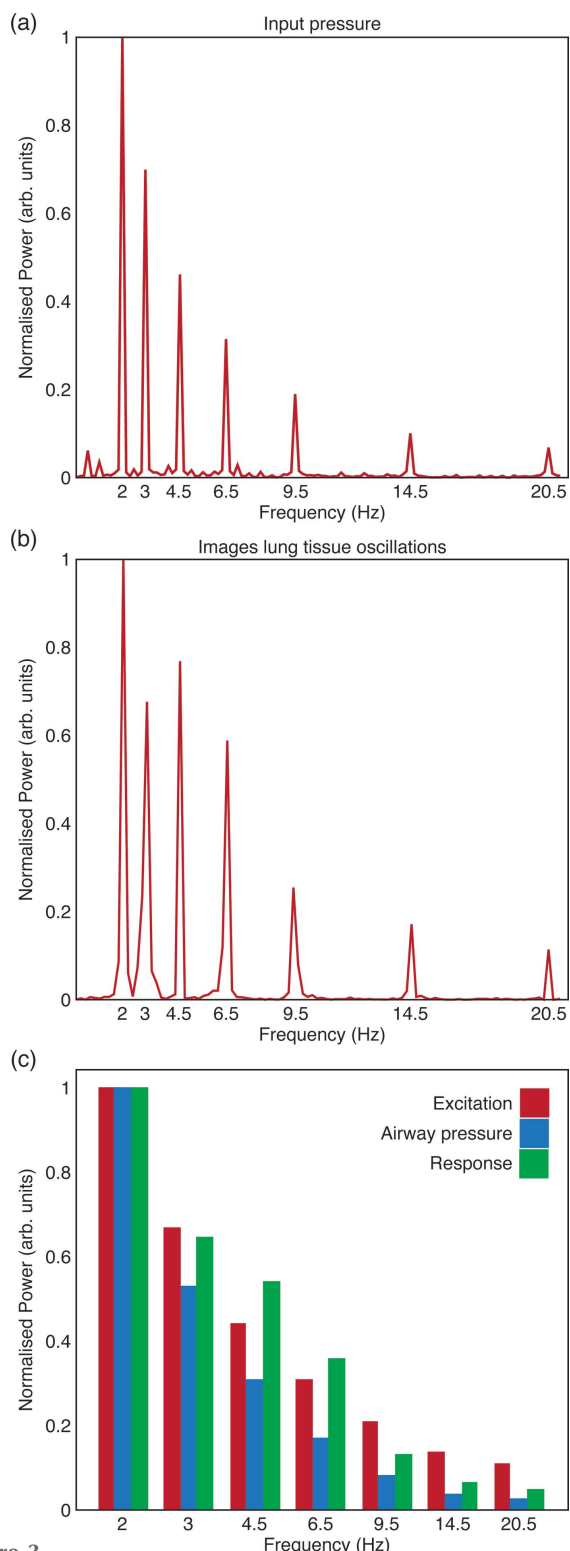
Figure 3
Frequency response of the respiratory system to an input signal applied at the airway opening. The response was measured *via* a pressure sensor at the airway opening (*a*) and by the novel imaging technique (*b*). The total power of the frequency responses was calculated by binning the data using a 1/6 octave band (*c*). As such we can see that there is a consistent pattern between the three different curves and that the lower peak at 2 Hz from (*b*) is no longer decreased relative to the other frequencies. Imaging measurements were integrated across the entire lung to produce a global measure equivalent to the measurement at the airway opening. All graphs were normalized to the power at the lowest input frequency.

(a)

(b)

Magnitude of tissue expansion
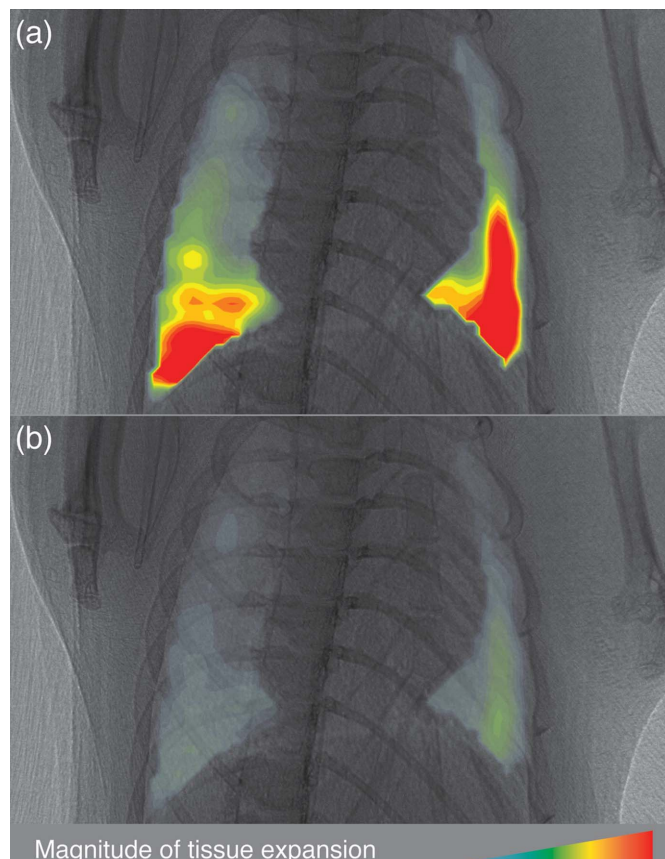
Figure 4
Distribution of lung tissue expansion occurring at 3 Hz (*a*) and 9 Hz (*b*) within the same mouse. The scale of the lung tissue expansion contour levels are arbitrary units and were normalized to the maximum power of tissue oscillation that occurred at the lowest input frequency.

frequency as well as at the frequency of the heart and its subsequent harmonics. The maps showing power of expansion oscillations were overlaid on an input X-ray image of the subject to provide an anatomical reference (Fig. 4). Maps showing power of the lung tissue expansion can be displayed for any specific frequency, yet were limited on the upper bound by the imaging rate used. The regional distribution of lung tissue oscillations can be thoroughly investigated from these maps.

3. Results

We were able to discriminate and quantify the frequencies and associated powers for each of the input pressure frequencies *via* this imaging technique (Fig. 3). The discrimination of the individual input frequencies was found to be accurate as a result of the temporal resolution of the imaging system. In addition to this, with increasing frequency a similar decline in power was observed for both the input pressure signal and the imaging-based measure (Fig. 3), demonstrating the fidelity of the imaging measurements.

At the lower frequencies it was found that the signal penetrated well into the base of the lung, yet only minimal signal was observed to be inducing oscillations of the lung

tissue in the apices (Fig. 4a). At the higher frequencies smaller oscillations were observed, as expected, yet a similar distribution of oscillations occurred between the base of the lung and the apex (Fig. 4b).

The data from the expansion maps were averaged across each row and then plotted against distance (in windows) from the apices, to determine the vertical distribution of input oscillations between the apices and base of the lung (Fig. 5a). The vertical distribution of oscillations resultant from the action of the heart and its harmonics appears to exist higher up in the lung (Fig. 5b). An increase in oscillations was observed in the base of the lung relative to the apices at all frequencies. Although the higher frequencies showed a decrease in the power of oscillations from the apices to the base, this effect was not as apparent as for the lower frequencies. This indicates a more uniform penetration of the input signal at higher frequencies when compared with lower frequencies.

The frequency response measured in one of the live animals showed a decrease in power at the lowest frequency, yet the decrease in power with increasing frequency was similar to the input signal. In addition to this trend, the frequency of the heart was seen at 6.87 Hz and its first harmonic at 13.74 Hz (Fig. 6). The attached ECG measured the heart rate at 6.7 Hz. It was observed from the maps of lung tissue expansion that there was considerable effect of the heart on surrounding lung tissue (Fig. 6).

4. Discussion

X-ray velocimetry measurements of lung tissue oscillations were found to agree well with the powers and frequencies imparted *via* a pressure oscillation signal applied at the airway opening. It has been demonstrated that this technique is capable of accurately mapping the distribution and the power

of lung tissue oscillations as a result of a pressure signal applied at the airway opening. For the first time, the penetrance of the input pressure oscillations was measured and mapped across the lung.

The maps of lung tissue oscillations (Fig. 6, right) indicate that even at the low frequencies the signal penetrates well into the base of the lung, yet limited signal penetrates to the apex of the lung. The distribution of lung tissue oscillations is equivalent to a map of the penetrance of the input oscillation signal. If the input oscillatory signal does not penetrate evenly to all regions of the lung, then lung tissue oscillations will not be observed in regions that the signal does not penetrate to. These regions that do not have any input signal penetrating to them presumably are not contributing to the measures of lung function that are being made at the airway opening. Under these circumstances the forced oscillation signals measured at the mouth are largely describing the lower portion of the lung and as a result may not truly be representative measures of the entire lung. This is an important finding because in lung disease there can be significant airflow obstruction and closure further limiting the amount of lung being measured.

Whilst the X-ray velocimetry measures were representative of the input oscillations, there was a decrease in power of the oscillations at the lower frequencies [Fig. 3(b) at 3 Hz and Fig. 6 at 2 Hz]. The frequency response data were analysed using binning of the 1/6 octave band to calculate the total power at each frequency taking into account any broadening of the peak. When this analysis was conducted, the various decreases in power at lower frequencies were no longer observed (Fig. 3c). As a result, the authors believe that these decreases in peak power are a result of resonance and, when accounting for the broadening of the peak, the total power at the frequencies is an exponential decay as expected. It should be noted that the tests were performed on both deceased (Fig. 3) and live (Fig. 6) animals. For the live animals, oscil-
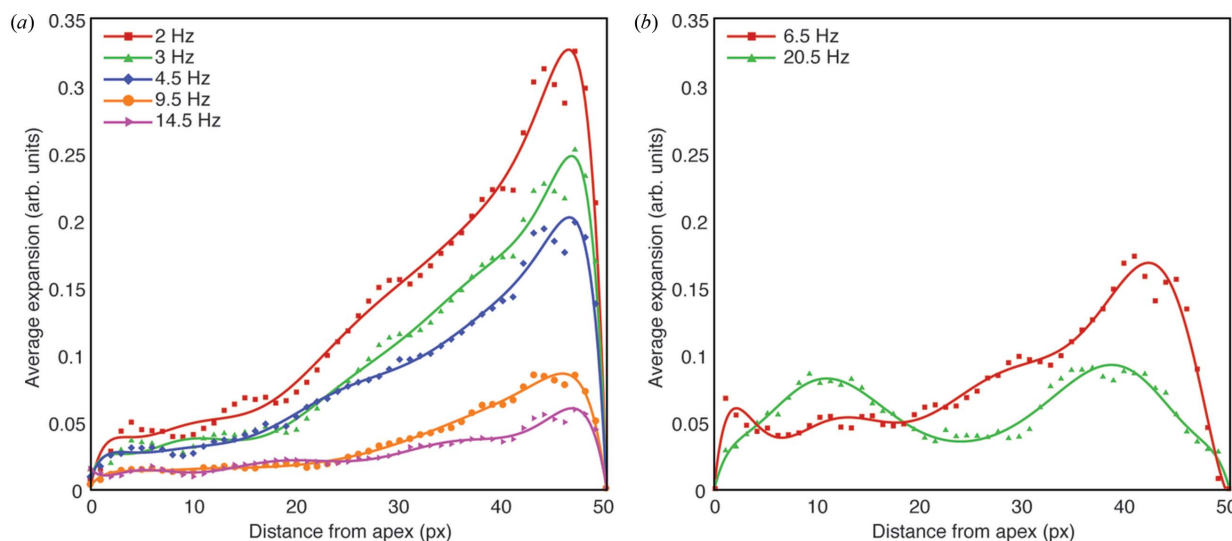
Figure 5
Vertical distribution of lung tissue oscillations for input frequencies (a) and for heart frequencies (b). The average expansion is calculated for each row of interrogation windows in the image analysis. Due to the frequency of the heart (6.87 Hz) and its second harmonic (20.3 Hz) there was interference with the 6.5 Hz and 20.5 Hz oscillations, therefore both curves have been omitted from this graph. There is a clear decrease in the expansion as the frequency increases. Also it can be seen that the vertical distribution of lung tissue oscillations is more uniform at the higher frequencies. See supporting information figures for the same data for the other animals, highlighting the consistent patterns that were seen across the three subjects.
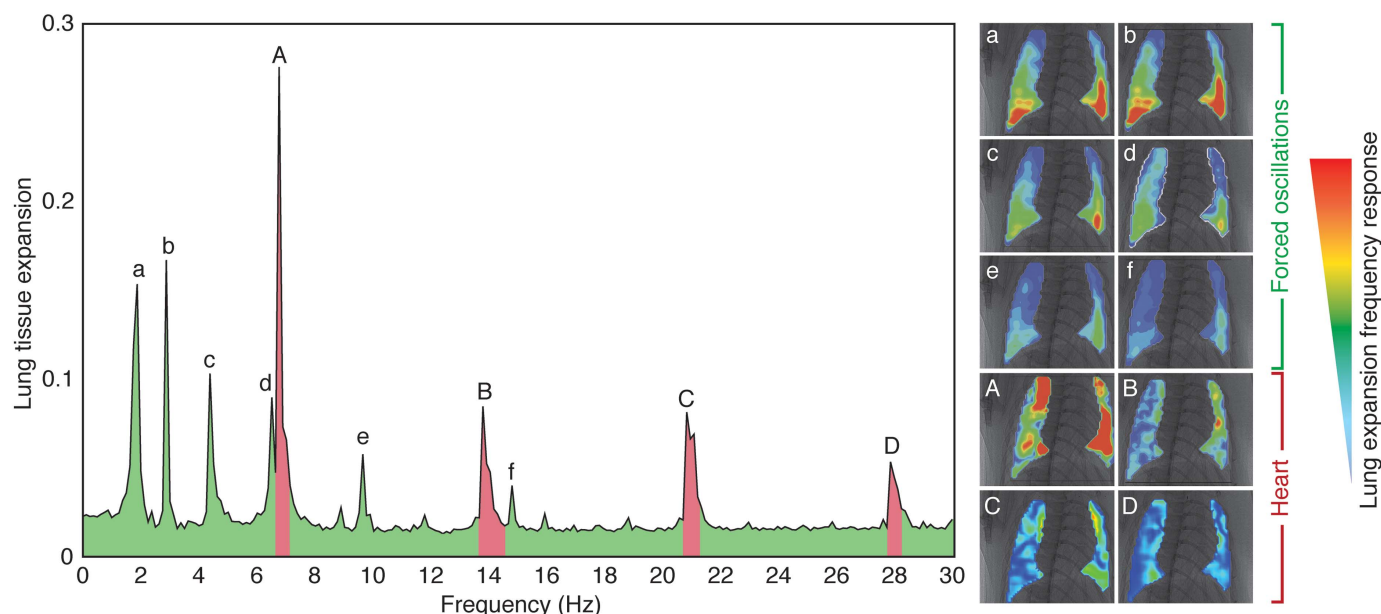
Figure 6
Frequency response (left) showing the power of lung tissue expansion (arbitrary units) summed across the lung. A peak exists at the frequency of the heartbeat (6.87 Hz) and the first harmonic of the heart frequency (13.74 Hz). The ECG measured the heart rate to be 6.7 Hz. We mapped the distribution of lung tissue oscillations at each input frequency and the heart frequencies across the lung (right). Contour levels showing magnitude of expansion in the lung maps are identical to the levels show in the legend in Fig. 4. These data show that the heart and the input pressure oscillations contribute to lung expansion within different regions of the lungs.

lations originating from the action of the heart can be observed in both the global frequency response and the maps of tissue oscillation at the heartbeat frequency (Fig. 6, A and B). Yet the use of imaging provides the ability to differentiate the heart's effect on different locations within the lungs. Due to the phase differences in lung tissue expansion caused by the action of the heart, any measures made at the airway opening would be susceptible to destructive interference, reducing the power of these signals when measured at the mouth. A recent publication has been able to demonstrate the existence of such internal oscillations in human subjects (Collier et al., 2015).

The expansion maps at frequencies that correspond to the heartbeat or its harmonics (Fig. 6; 6.87 Hz and 13.74 Hz, respectively) exhibited expansion that occurs in regions most proximal to the heart. It was seen that in the locations of the ventricles and the atria there was significant tissue oscillations (Fig. 6, A and B). The amplitude of lung tissue motion that resulted from the physical action of the heart was considerably larger than the lung tissue oscillations created from the input pressure signal. Several of the animals displayed a broad peak at the frequency of the heart that often resulted in significant interference when the heart rate was similar to one of the input oscillation frequencies. A broad peak on the frequency spectrum at the frequency of the heart indicates variability in the heart rate throughout the test. This highlights the ability of these imaging and image-processing methods to quantify not only externally applied oscillations but also internally generated oscillations.

As these animals were in the upright position during imaging, gravity may have an effect on the distribution of the forced oscillation signals throughout the lungs as gravity is known to affect the lungs (Hopkins et al., 2007). It would be

highly informative to understand how signal penetrance changes throughout the lung due to varied postures of the subjects, though this requires further technical developments to be made in terms of the imaging setup and animal handling. Throughout this study the subjects were imaged in the upright position due to practical constraints on the experimental setup.

It is not clear how the X-ray velocimetry measurements relate to the individual parameters of the single compartment mathematical models. However, we hypothesize that an X-ray velocimetry expansion measure would predominantly correlate to a tissue elastance (H), as this describes the frequency-dependent elastic behaviour of the system. Although a constant phase model was used for the forced oscillation analysis, a more complex analysis investigating the phase shifts is possible for the measures at the airway opening and theoretically could also be completed using this imaging technique. Such an analysis could shed further insight on the quality and accuracy of measurements that are being made only at the airway opening. Nevertheless, it becomes apparent from this work that under these conditions the forced oscillation input pressure signal does not penetrate evenly throughout the lung.

In conclusion, using novel image-processing methods in combination with X-ray velocimetry we identified and quantified the power of lung tissue oscillations on a regional basis across the entire lung at each of the input frequencies of a standard forced oscillation test in mice. Observations indicate that the signal may penetrate well into the base of the lung, yet minimal tissue oscillations were measured in the apices. This technique has the potential to determine the exact mechanisms by which forced oscillation techniques measure global lung function and thus allowing for the development of more

advanced and effective forced oscillation signals. Research into the effects of different frequency ranges as well as the phase shifts of the signals will enable these further developments. Further studies involving larger numbers of subjects should now be completed to answer the complex biomedical questions relating to heterogeneity of input oscillation signals as well as the effects of resonance in the mouse lung. The work presented here has established the technique that can serve as the tool for such large biomedical studies.

References

Antoine, E., Buchanan, C., Fezzaa, K., Lee, W.-K., Rylander, M. N. & Vlachos, P. (2013). *PLoS One*, **8**, e81198.

Bates, J. H. T., Irvin, C. G., Farré, R. & Hantos, Z. (2011). *Comprehensive Physiology*. New York: John Wiley and Sons.

Bates, J. H. T. & Suki, B. (2008). *Respir. Physiol. Neurobiol.* **163**, 54–63.

Collier, G. J., Marshall, H., Rao, M., Stewart, N. J., Capener, D. & Wild, J. M. (2015). *J. Appl. Physiol.* **119**, 1007–1014.

Dubsky, S., Hooper, S. B., Siu, K. K. & Fouras, A. (2012). *J. R. Soc. Interface*, **9**, 2213–2224.

Dubsky, S., Jamison, R. A., Irvine, S. C., Siu, K. K. W., Hourigan, K. & Fouras, A. (2010). *Appl. Phys. Lett.* **96**, 023702.

Fouras, A., Allison, B. J., Kitchen, M. J., Dubsky, S., Nguyen, J., Hourigan, K., Siu, K. K., Lewis, R. A., Wallace, M. J. & Hooper, S. B. (2012). *Ann. Biomed. Eng.* **40**, 1160–1169.

Fouras, A., Kitchen, M. J., Dubsky, S., Lewis, R. A., Hooper, S. B. & Hourigan, K. (2009). *J. Appl. Phys.* **105**, 102009.

Frantz, I. D. & Close, R. H. (1985). *Pediatr. Res.* **19**, 162–166.

Fredberg, J. J., Keefe, D. H., Glass, G. M., Castile, R. G. & Frantz, I. D. (1984). *J. Appl. Physiol.* **57**, 788–800.

Hantos, Z., Daroczy, B., Suki, B., Nagy, S. & Fredberg, J. J. (1992). *J. Appl. Physiol.* **72**, 168–178.

Hopkins, S. R., Henderson, A. C., Levin, D. L., Yamada, K., Arai, T., Buxton, R. B. & Prisk, G. K. (2007). *J. Appl. Physiol.* **103**, 240–248.

Jamison, R. A., Siu, K. K. W., Dubsky, S., Armitage, J. A. & Fouras, A. (2012). *J. Synchrotron Rad.* **19**, 1050–1055.

Kitchen, M., Habib, A., Fouras, A., Dubsky, S., Lewis, R., Wallace, M. & Hooper, S. (2010). *J. Instrum.* **5**, T02002.

Kitchen, M., Paganin, D., Lewis, R., Yagi, N., Uesugi, K. & Mudie, S. (2004). *Phys. Med. Biol.* **49**, 4335–4348.

Komarow, H. D., Myles, I. A., Uzzaman, A. & Metcalfe, D. D. (2011). *Ann. Allergy Asthma Immunol.* **106**, 191–199.

Larcombe, A. N., Zosky, G. R., Thamrin, C., Bozanich, E. M., Hantos, Z. & Sly, P. D. (2013). *Influenza Other Respir. Viruses*, **7**, 889–894.

Lee, W.-K., Fezzaa, K. & Uemura, T. (2011). *J. Synchrotron Rad.* **18**, 302–304.

Lewis, R., Yagi, N., Kitchen, M., Morgan, M., Paganin, D., Siu, K., Pavlov, K., Williams, I., Uesugi, K., Wallace, M., Hall, C. J., Whitley, J. & Hooper, S. B. (2005). *Phys. Med. Biol.* **50**, 5031–5040.

Momose, A., Takeda, T., Itai, Y. & Hirano, K. (1996). *Nat. Med.* **2**, 473–475.

Oostveen, E., MacLeod, D., Lorino, H., Farré, R., Hantos, Z., Desager, K. & Marchal, F. (2003). *Eur. Respir. J.* **22**, 1026–1041.

Seeger, A., Affeld, K., Goubergrits, L., Wellnhofer, E. & Kertzscher, U. (2001). *Exp. Fluids*, **31**, 193–201.

Thurgood, J., Dubsky, S., Henon, Y., Jesudason, E. & Fouras, A. (2014). *American Thoracic Society International Conference Abstracts*, A6275. American Thoracic Society.

Thurgood, J., Dubsky, S., Siu, K. K. W., Wallace, M., Siew, M., Hooper, S. & Fouras, A. (2012). *Proc. SPIE*, **8506**, 85060H.

Thurgood, J., Hooper, S., Siew, M., Wallace, M., Dubsky, S., Kitchen, M., Jamison, R. A., Carnibella, R. & Fouras, A. (2012). *PLoS One*, **7**, e48122.

Zosky, G. R. & Sly, P. D. (2007). *Clin. Exp. Allergy*, **37**, 973–988.